

1 Article

2 Non Linear Strain Measures on Concrete Structures 3 by Means of Embedded Optical Fiber Sensors

4 Vincenzo Minutolo ^{1,*}, Renato Zona ¹

5 ¹ Department of Engineering, University of Campania, "Luigi Vanvitelli" , via Roma, 81031 Aversa, Italy

6 * Correspondence: vincenzo.minutolo@unicampania.it;

7

8 **Abstract:** Optical fiber sensors have become a widely-used tool to perform life-long monitoring of
9 large structures. Different set-ups of sensors can be used to obtain information at different scopes.
10 In this paper, the application of a portable Brillouin optical time domain analysis sensor applied to
11 reinforced concrete beams is presented. The sensor is made up of a single-mode optical fiber applied
12 to the structure that enables the measurement of tensile and compressive axial strain along the
13 beams. The fiber is embedded into a concrete casting and fixed along the reinforcement bars so that
14 a complete correlation can be obtained regarding strain and displacements in linear and non-linear
15 flexural response. The use of four sensing fibers positioned along the beam's length at different
16 vertical positions makes it possible to read the strain variation within the cross-section. In
17 accordance with Bernoulli's hypothesis, this allows curvature diagrams to be obtained across the
18 structure. The measured curvature is used to set up the moment–curvature relationship, which
19 highlights the possibility of the sensor monitoring structures continuously in space and time.

20 **Keywords:** Concrete structures, structure monitoring, optical fiber sensors, distributed sensors,
21 Brillouin scattering.

22

23 1. Introduction

24 The basis of structural health monitoring (SHM) has been laid by Housner et al. [1], where it is defined
25 as the continuous measurement and analysis of the main structural and environmental parameters
26 under operating conditions in order to detect anomalous behavior in the initial phases and then as a
27 prevention tool.

28 The health monitoring of structures is therefore necessary, so that during the design phase and during
29 construction the structures can be equipped with opportune sensors and suitable monitoring process
30 could be projected especially as an integral part of preventive maintenance procedures in service and
31 in the assessment of damages.

32 The methods for SHM in materials and structures include ultrasonic testing [2,6], thermography [7,9]
33 and measurements of static deformation and dynamic vibrations [10,13]. Static stresses and dynamic
34 vibration analysis are often limited to the reading of point sensors, such as strain gauges,
35 accelerometers [1] or contactless laser, Doppler vibrometers [14,15].

36 Distributed strain measurements using optical fiber sensors has great advantages with respect
37 to measurements done by traditional gauges such as resistive or mechanical ones, and among others
38 those based on Brillouin optical time domain analysis (BOTDA) that are discussed here. The optical
39 fiber plays the role of a sensor and also of the communication medium and is very cheap since the
40 sensor is made of nothing but data transmission fiber. The feasibility of this kind of sensor is
41 particularly suitable to concrete and other structures in Civil Engineering; the construction process,
42 indeed, consists of several phases in a very unclean environment and is subjected to severe shocks
43 and manipulation that can damage the sensor. In many papers, a detailed review of optical fiber
44 sensors is presented where the properties of BOTDA sensors are described; it can be seen that the use
45 of a distributed sensor has great advantages with respect to the installation economy, set-up design

46 and realization and data acquisition. Several experiments, as described in [16, 17], show that
47 building activity often damages electrical strain gauges or vibrating wire deformometers. In practice,
48 structures are investigated experimentally only at the completion of construction, during final
49 testing, when gauges are applied for a short elapsing time, whereas the life-long monitoring of the
50 finished structure is not as frequently performed as it should be. As a matter of fact, life-long
51 measurement is the new challenge in Civil Engineering, especially with respect to construction
52 maintenance and management. It is clear that life-long monitoring requires that the sensors are
53 positioned in situ and left in place for a long time; consequently, they need to be protected from the
54 injuries caused by time and their environment [18].

55 Optical fibers for telecommunications, which are the sensing devices when BOTDA is used, are very
56 robust and do not suffer time degradation, but the fiber is rather fragile and requires some protection
57 against mechanical shocks. For the scope, it is desirable that the fiber is protected by means of coating
58 or by embedding the fiber itself into the concrete cast. An experimental arrangement that places
59 embedded fibers into concrete structures is presented in several works where the feasibility of such
60 a set-up is shown [19, 23].

61 Barrias and Bao [24, 25] describe the evolution of the SHM with a review of the major experiments
62 and results carried out to date to demonstrate the effectiveness of the use of optical fiber sensors.

63 Several experiments have been performed in the BOTDA field with embedded sensors for different
64 types of structures: reinforced concrete wall [26], prestressed concrete bridge [27], integrated optical
65 fiber in functionalized carbon structures (FCS) [28] and also for the detection of vibration, surface
66 cracking and buckling phenomena [29, 31] in reinforced concrete, pre-stressed concrete (PSC) [32]
67 and post-tensioned PSC [33].

68 In the present work, laboratory experiments are presented that concern reinforced concrete beams
69 under flexural solicitation; the structures have been instrumented by embedded optical fibers, and
70 the experimental configuration has been set up in order to account for the Bernoulli beam theory.

71 The sensor consists of a Stimulated Brillouin Scattering portable prototype based on Brillouin Optical
72 Time-Domain Analysis (BOTDA). This type of analysis makes use of a pulsed laser light and a
73 frequency-shifted continuous-wave light, which are launched at the two opposite ends of an optical
74 fiber that serves as the sensing element. The intensity of the light emerging from the fiber at various
75 frequency shifts is recorded and the recorded profile along the fiber is retrieved. Since the linear
76 dependence of the Brillouin frequency shift on strain, the instrument provides a measure of strain at
77 each location of the fiber, with a spatial resolution determined by the duration of the optical pulses
78 employed for the measurements. More detail on the equipment can be found in [34-37] where some
79 application of the sensor is described with reference to other structures.

80 It is shown that the embedded fiber sensor is able to reconstruct beam cross-section deformation;
81 hence, curvature mapping is obtained along the whole beam with very little effort and a cheap cost.

82 In the following, a number of experimental measurements are reported. The experiments concern a
83 set of four laboratory beams made of reinforced concrete. The beams have been loaded by two point
84 forces, placed to obtain a large zone where pure bending alone acts as internal solicitation.
85 Consequently, the beams have presented a pure bending failure, with a small influence of the shear
86 on the collapse, as shown by the crack patterns recorded at the end of each test.

87 The experimental results show that the sensor is able to follow the load path from a low load level
88 until plastic collapse. For this target, the beams have been instrumented by using four optical fibers
89 at different heights along the structure. The curvature of the deformed shape of the beams is
90 calculated by the variability of longitudinal strain along the height, in accordance with Bernoulli
91 theory. As was expected, the actual deformation of the beam's cross-section remains almost planar,
92 even at the non-linear stage of the stress. This result confirms the possibility of this kind of sensor
93 being able to monitor ultra-elastic deformation.

94 By the result here presented, one can see that the strain map within the cross section of the beam is
95 reconstructed properly. This confirms that the measured strain, within admissible approximation, is
96 accurate enough, although the fiber is embedded into concrete cast without particular precautions.

97

98 2. Materials and Methods

99 Laboratory experiments have concerned reinforced concrete (RC) beams, casted by using
100 designed concrete in order to obtain the prescribed of resistance $f_{ck} = 25MPa$. **Figure 1** shows the
101 casting phase, the reinforcement pattern and the fiber positioning. The beam shape is summarized
102 hereafter:

103 The length of the beam span is $l = 1.82m$, the beam has square cross section with side length
104 $b = 0.20m$. The reinforcement consists of four longitudinal steel bars, at the vertex of the beam; the
105 bars have diameter $\phi_l = 12mm$. Finally, eight steel brackets whose diameter is $\phi_b = 8mm$
106 complete the reinforcement. The sensing device has been designed to monitor the axial strain within
107 the beam at different locations along the longitudinal directions and at different vertical positions.
108 Then, it has been possible to get the longitudinal curvature of the beam axis provided by Bernoulli's
109 hypothesis to hold; for the scope, each beam has been instrumented by coiling a single optical fiber
110 four times along the whole beam's length. The sensor disposition allowed us to record four strain
111 patterns at different heights. The fiber has been glued to the brackets and along the longitudinal bars
112 by epoxy resin; moreover, a grid made of iron wires has been applied through the brackets so that
113 the optical fiber could be suspended at the prescribed position, as depicted in **Figure 1**.
114



Figure 1. Fiber fixing: (a) the upper fiber is glued to the reinforcement; (b) an iron wire grid to fix the lower fibers.

115 It has to be stressed that the fibers is not glued to the structure mass but simply embedded. The
116 connection with the concrete is checked by the accuracy of the curvature reconstruction that has been
117 obtained during the experiments. As a result, we confirm that simply embedded fibers can measure
118 concrete strain with sufficient accuracy.



Figure 2. Testing apparatus, load frame and hydraulic jacks

119 The loading equipment, as shown in **Figure 2**, consists of a steel frame, where rolling cylindrical
 120 supports are positioned at the testing span distance, in order to provide the supports that allow
 121 horizontal displacements. Hence, the beam is subjected only to transversal actions (i.e. zero axial
 122 force).
 123 The transversal position of the fibers is represented in **Figure** , where the structural scheme of the
 124 specimen is drawn as well.
 125 The fiber position along the section height, measured from the bottom of the beam, is shown in the
 126 following **Table 1**.

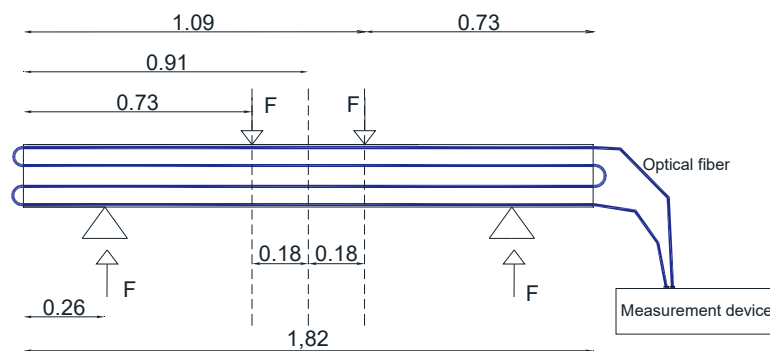


Figure 3. Testing scheme with fiber positions.

127 The load has been applied by means of two hydraulic jacks whose position is depicted in **Figure** . The
 128 experiment has been designed so that, at the middle of the beam span, constant bending moment
 129 results; such a loading pattern allows us to decouple the bending failure mechanism from shear
 130 effects.

131 **Table 1.** Position of the fiber sensors measured from the bottom.

Fiber n.	Distance from bottom
	mm
1	160
2	126
3	74
4	20

132 In order to have a redundant control of the electronic measures, the structure has been equipped
 133 with a displacement dial gauge, positioned at the middle span of the beam, as represented in **Figure**
 134 **4**.



Figure 4. Dial displacement gauge position.

135 During the experiment, a time variable load has been applied through the servo-controlled jacks. The
 136 load program consists of a prescribed set of loading–unloading steps.
 137 The structure has been tested with respect to bending, where the loads have been applied so that the
 138 bending moment was the main internal stress. Under such hypotheses, the main strain of the
 139 structure is the longitudinal one, ε ; under these conditions, the optical fibers give better results.
 140 The analytical solution of the collapse of the beam is obtained according to the reinforced concrete
 141 homogenization theory and to the prescription of Eurocode 2 (EC2).

142 3. Results

143 The constitutive mechanical parameter of the concrete is yield stress:

$$144 \quad \sigma_{cy} = 13.75 \text{ MPa} \quad (1)$$

145 The concrete is assumed no-tension resistant with limited ductility; hence, the stress–strain
 146 relationship is defined in the compression range and vanishes at large strain,

$$147 \quad \begin{aligned} \sigma_c &= 0 & , \varepsilon < -0.0035 \\ \sigma_c &= \sigma_{cy} & , -0.0035 < \varepsilon < -0.002 \\ \sigma_c &= (1000\sigma_y)\varepsilon + (250000\sigma_y)\varepsilon^2 & , -0.002 < \varepsilon < 0 \end{aligned} \quad (2)$$

148 On the tensile range the stress vanish as well.

149 The steel of the bars is supposed to be an elastic, perfectly plastic material with a Young's
 150 modulus $E_s=210 \text{ GPa}$ and stress yielding at

$$151 \quad \sigma_{sy} = 380 \text{ MPa}$$

152 The stress–strain curve for the steel has the following expression:

$$153 \quad \begin{aligned} \sigma_s &= 0 & , \varepsilon < -0.01 \\ \sigma_s &= -\sigma_{sy} & , -0.01 < \varepsilon < -0.002 \\ \sigma_s &= E_s \varepsilon & , -0.002 < \varepsilon < 0.002 \\ \sigma_s &= \sigma_{sy} & , 0.002 < \varepsilon < 0.01 \\ \sigma_s &= 0 & , 0.01 < \varepsilon \end{aligned} \quad (3)$$

154 The stress strain curves for the two materials are drawn in **Figure 5**.

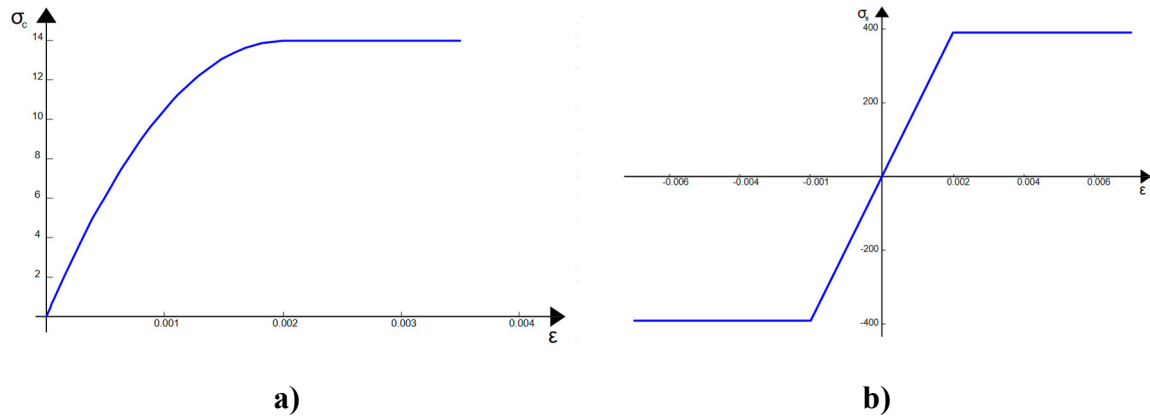


Figure 5: stress strain curves of the materials, a) concrete, b) steel

155 By means of the above definitions, equations (2) and (3), the moment curvature is obtained by
 156 prescribing a curvature value, assuming that the neutral axis is horizontal and in such a position that
 157 divide the cross section in two parts where the stress resultants are opposite. Finally, by integrating
 158 the stress moment about the neutral axis along the beam thickness, one can calculate the moment-
 159 curvature relationship. The moment-curvature diagram is drawn in **Figure** .

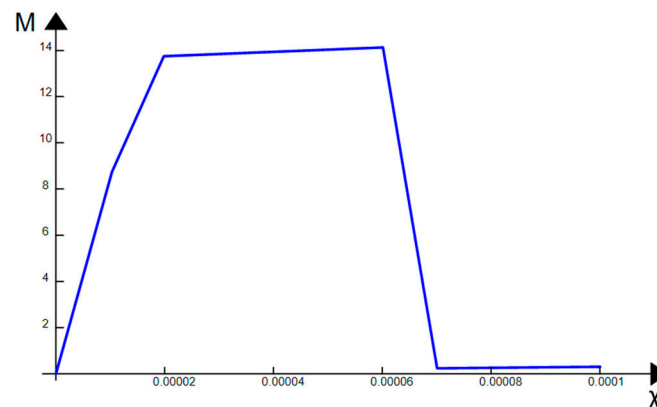


Figure 6: Bending moment versus curvature diagram

160 The maximum moment calculated using the described procedure is:

$$161 \quad M_m = 14.20 \text{ kNm} \quad (4)$$

162 An analogous calculation, made by means of standard formulas in European code EC2, gives
 163 the following results (see Table 2) that are in a rather good accordance with those reported above.

164 Table 2: Mechanical properties of the RC beam cross section by EC2.

Item	Value
Limit moment	13.9 kNm
Limit neutral axes y_n^p	0.168 m
Elastic neutral axes y_n^e	0.14 m
Upper ε	.0021
Lower ε	.01

165

166 where Upper ε and Lower ε stand for strain at the upper—i.e. most compressed—and lower—i.e.
 167 most tensed—side of the structure; y_n^p and y_n^e are the distances of the neutral axis from the bottom
 168 of the beam when complete plastic strain occurs and at the elastic limit, respectively.

169 The theoretical value of the limit moment allows us to calculate the limit load, as

$$M_y = F_y d \Leftrightarrow F_y = \frac{M_y}{d} \quad (5)$$

170 By using the quantity reported in Figure 3, one obtains

$$d = 0.73m - 0.26m = 0.47m$$

$$F_y = \frac{13.9kNm}{0.47m} = 29.6kN \quad (6)$$

171 A typical record of strain obtained during the experiments is reported in Table 3. The diagram,
 172 depicted in Figure 7, consists of several three curves, one for any loads step, each of them can be
 173 divided into four fields (one can see four waves representing the fields) that represent the strains
 174 along the optical fiber for the different span paths. Since the length of the portion of the fiber that is
 175 embedded into the beam is known *a priori*, it is possible to relate the abscissa to the relevant cross-
 176 section and height within the beam. Hence, the strain shown in figure 7 actually represents a two-
 177 dimensional map of the strain over the beam.

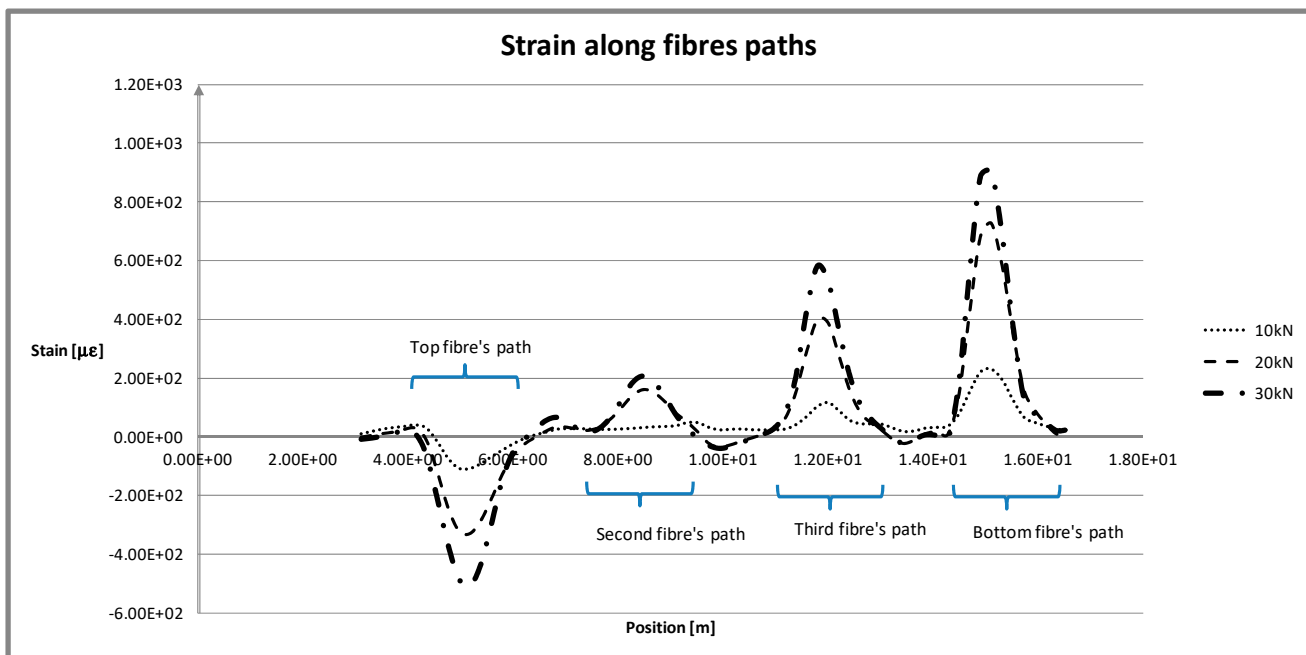


Figure 7: Strain recording along the fiber for different load steps

178 In the following Table 3, the strains at sections located at the mid-span of the beam, i.e. at a distance
 179 z from the left-wise support given by $z = 0.91m$ (see Figure 3), are reported; in the table, the beam
 180 curvature and bending moment, calculated analytically from recorded data, are reported as well. By
 181 assuming that the Bernoulli hypothesis on the plane cross-section holds, the curvature is calculated
 182 by

$$\chi = \frac{\varepsilon_l - \varepsilon_u}{h - c}, \quad (7)$$

183 where $h - c$ is the distance from the fibers along the cross-section height, $c = 20mm$ is the
184 distance of the bars from the upper and the lower side of the section and h is its height.

185 **Table 3.** Results at mid span: $z = 0.91$ m.

Force [KN]	Lower ε	Upper ε	Curvature χ [1/m]	Moment [KN m]
0	0	0	0	0
10	0,000378	-0,0000516	0,002685	4,7
20	0,000837	-0,000082	0,00574375	9,4
30	0,00127	-0,000142	0,008825	14,1
40	0,00218	-0,000178	0,0147375	18,8
50	0,00476	-0,000225	0,03115625	23,5
40	0,00477	-0,000177	0,03091875	18,8
30	0,0058	-0,0000894	0,03680875	14,1
20	0,00733	0,0000021	0,04579938	9,4
10	0,00665	0,000226	0,04015	4,7
2	0,00641	0,000367	0,03776875	0,94

186 The theoretical limit response of the beam, as summarized in Table 2 and the limit load
187 calculated in equation(6), allows us to notice that the conventional limit suggested by EC2 is lower
188 than the measured limit. This result confirms that the conventional limit does not represent the actual
189 behavior of the structure. The same comment holds with respect to the prescribed limit strain to be
190 used in analytical calculation; more precisely, the standard resistant moment is assumed to
191 correspond to the prescribed strain limits, which are reported in Table 2, even if these limits do not
192 conform to the actual response of the structure.

193 The moment–curvature ($M - \chi$) diagram, **Figure 9**, is drawn from recorded data; Table 3
194 reports the results concerning the cross-section at the middle of the beam span during the loading
195 and unloading phases of the last load step, and analogous results have been elaborated in order to
196 obtain the $M - \chi$ diagram for various cross-sections. In particular, in the following Figure, three
197 significant diagrams are reported corresponding to the point where the force has been applied, the
198 mid-span point and a point outside the load application range. The diagrams related to $z=0.73m$ and
199 $z=0.91m$ are almost equal, thus confirming that, within the beam portion between the two acting
200 forces, the moment is actually constant; moreover, one can see that the diagrams account for the snap
201 back discontinuity of the moment, indicating that sudden cracks grow together with a non-linear
202 occurrence. The diagram indicated by $z=1.26m$ refers to the point where the bending moment is less
203 than the yield limit, although it is greater than the first crack growth limit. From the diagram, it can
204 be seen that the curvature does not recover anymore at unloading, but no sudden decrease of the
205 stress occurs, since it has to be expected that only micro-cracks develop at this stage. Finally, it can
206 be seen, from any of three diagrams, that the linear part of the moment–curvature law is well
207 recorded by the measurement device with a good agreement with theoretical expected values.

208 In order to check the measured strain during the non-linear response of RC beams, a comparison
209 with the theoretical prediction has been reported hereafter.

210 For the scope, the actual neutral axis elevation with respect to the beam bottom line has been
211 calculated by strain measures, both in elastic and plastic phases, y_n^e and y_n^p . In any case, the actual
212 neutral axis elevation y_n depends on strain by means of the following linear equation:

$$y_n = c + \frac{\varepsilon_l}{\varepsilon_l - \varepsilon_u} (h - c) \quad (8)$$

213 Equation (8) has been used to obtain y_n during several load steps; in particular, the measurements
 214 have been permitted to calculate y_n during the last monotone load path. The results are
 215 summarized in the following table (Table 4), and it can be seen that the neutral axis has moved
 216 upwards during crack propagation and non-linear strain occurrence.

217

Table 4. Neutral axis translation from elastic to plastic.

F	ε_l	ε_u	y_n
10	0.00038	-5.16E-05	0.160782
20	0.00084	-0.000082	0.165724
30	0.00127	-0.000142	0.163909
40	0.00218	-0.000178	0.167922
50	0.00476	-0.000225	0.172778

218 Such a behavior can be ascribed to the fact that the stress does not remain elastic anymore, and hence
 219 its result increases with respect to the linear case.

220 The beam is under elastic load for $F = 10kN$ and the neutral axis has the following elevation:
 221

$$y_n^e = 0.02 + \frac{0.00038}{0.00038 + -5.16 \times 10^{-05}} 0.16 = 0.161m \quad (9)$$

222 The value of y_n^p in the plastic stage is calculated for $F = 50kN$ and is obtained by equation(8),
 223 hence



Figure 8: Cracks at the incoming collapse

$$y_n^p = 0.02 + \frac{0.00476}{0.00476 + 0.000225} 0.16 = 0.173m \quad (10)$$

This result can be compared with the theoretical one, equation (4), and that obtained by EC2 and reported in Table 2. The strain measurements obtained by means of the optical fiber sensor allow us to calculate the function of the curvature of the beam along its span; the curvature χ has been calculated by equation (7) and the bending moment by equation (5).

Figure clearly shows that, at incoming collapse, the beam presents several cracks. The ruptures are of two types: the one at the lower edge of the structure consists of a crack that has to be imputed to the attainment of the tensile limit of the concrete; the other one, on the upper side of the beam, is due to the buckling of the compressed side outside the confined core of the beam by the brackets.

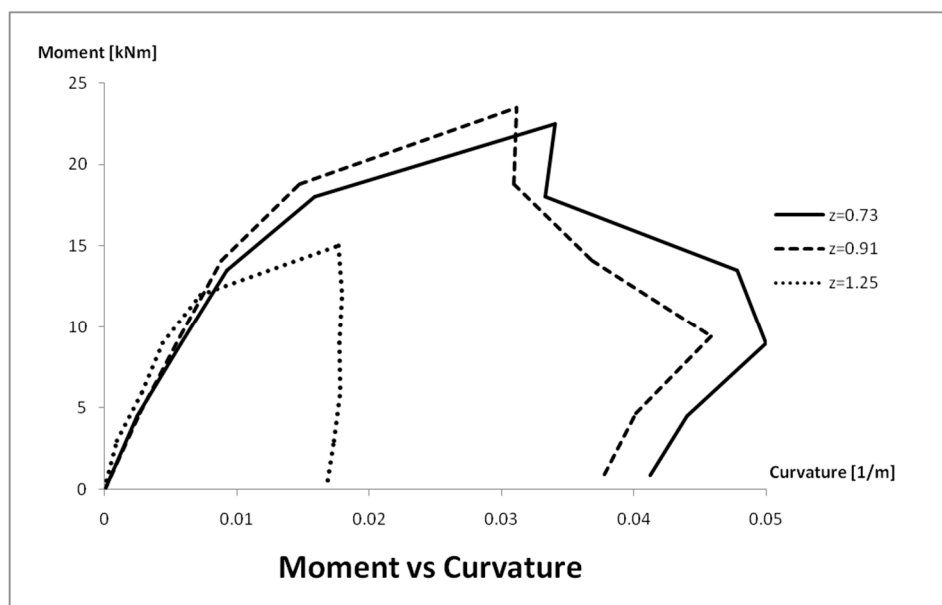


Figure 9. Moment–curvature diagrams for $z=0.73$, $z=0.91$, $z=1.25$ cross-sections.

5. Conclusions

The experiments reported have confirmed that Brillouin optical time domain analysis sensors can be used in civil engineering activities for structural monitoring. The experiments described in the present work, concern laboratory structures instrumented with ordinary optical fibers for telecommunication. The fibers are very cheap and easy to set up as a sensor, and they make it possible to set up complicated sensor lattices with little effort in terms of time and resources.

A particular set-up has been tested: it is made of a single fiber that runs within the beam along four different paths at different heights. The fiber is embedded into the concrete during its casting and is supported by means of a light iron cable tensed between the steel brackets and the reinforcement bars.

The experimental setup has been designed to obtain results on the strain distribution within the structure in order to give information both on the feasibility of accurate internal measurement and on the actual strain distribution within concrete beams at non-linear—for instance, fracture and plasticity—stress levels. Moreover, the experiment confirms that the fiber did not break during installation, even if no particular attention has been paid to avoiding damaging the sensor; only an ordinary cure has been applied. Hence, the sensor has shown its robustness with respect to damage at installation stage.

Moreover, it has been shown that the strain measurements obtained by means of BOTDA sensors can be used to get a continuous record along the structure and during the load time history with very

11. D. D. Rizos, S. D. Fassois, Z. P. Marioli-Riga and A. N. Karanika, "Vibration-based skin damage statistical detection and restoration assessment in a stiffened aircraft panel," *Mechanical Systems and Signal Processing*, **2008**.
12. C. Ratcliffe, D. Heider, R. Crane, C. Krauthauser, M. K. Yoon and J. W. Gillespie, "Investigation into the use of low cost MEMS accelerometers for vibration based damage detection," *Composite Structures*, **2008**.
13. T. H. Loutas, A. Panopoulou, D. Roulias and V. Kostopoulos, "Intelligent health monitoring of aerospace composite structures based on dynamic strain measurements," *Expert Systems with Applications*, **2012**.
14. Y. Zou, L. Tong and G. P. Steven, "Vibration-based model-dependent damage (delamination) identification and health monitoring for composite structures - a review," *Journal of Sound and Vibration*, **2000**.
15. A. Katunin, "Vibration-based spatial damage identification in honeycomb-core sandwich composite structures using wavelet analysis," *Composite Structures*, **2014**.
16. C.-Y. Hong, J.-H. Yin and Y.-F. Zhang, "Deformation monitoring of long GFRP bar soil nails using distributed optical fiber sensing technology," *Smart Materials and Structures*, **2016**.
17. X. Huang, M. Yang, L. Feng, H. Gu, H. Su, X. Cui and W. Cao, "Crack detection study for hydraulic concrete using PPP-BOTDA," *Smart Structures and Systems*, **2017**.
18. M. Fajkus, J. Nedoma, P. Mec, E. Hrubesova, R. Martinek and V. Vasinek, "Analysis of the highway tunnels monitoring using an optical fiber implemented into primary lining," *Journal of Electrical Engineering*, **2017**.
19. Y. Stern, Y. London, E. Preter, Y. Antman, H. Diamandi, M. Silbiger, G. Adler, E. Levenberg, D. Shalev and A. Zadok, "Brillouin optical correlation domain analysis in composite material beams," *Sensors (Switzerland)*, **2017**.
20. H. Mohamad, A. B. H. Kueh and A. S. A. Rashid, "Distributed optical-fibre strain sensing in reinforced concrete structures," *Jurnal Teknologi*, **2015**.
21. X. Feng, J. Zhou, C. Sun, X. Zhang and F. Ansari, "Theoretical and Experimental Investigations into Crack Detection with BOTDR-Distributed Fiber Optic Sensors," *Journal of Engineering Mechanics*, **2013**.
22. X. Zhao, P. Gong, G. Qiao, J. Lu, X. Lv and J. Ou, "Brillouin corrosion expansion sensors for steel reinforced concrete structures using a fiber optic coil winding method," *Sensors*, **2011**.
23. Z. S. Wu, B. Xu, T. Takahashi and T. Harada, "Performance of a BOTDR optical fibre sensing technique for crack detection in concrete structures," *Structure and Infrastructure Engineering*, **2008**.
24. A. Barrias, J. R. Casas and S. Villalba, "A Review of Distributed Optical Fiber Sensors for Civil Engineering Applications," *Sensors*, **2016**.
25. X. Bao and L. Chen, "Recent progress in Brillouin scattering based fiber sensors," *Sensors*, **2011**.
26. J. E. Woods, D. T. Lau, X. Bao and W. Li, "Measuring strain fields in FRP strengthened RC shear walls using a distributed fiber optic sensor," *Engineering Structures*, **2017**.
27. P. Banerji, S. Chikermane, K. Grattan, S. Tong, F. Surre and R. Scott, "Application of fiber-optic strain sensors for monitoring of a pre-stressed concrete box girder bridge," *2011 IEEE SENSORS Proceedings*, **2011**.

28. K. Bremer, F. Weigand, Y. Zheng, L. Alwis, R. Helbig and B. Roth, "Structural Health Monitoring Using Textile Reinforcement Structures with Integrated Optical Fiber Sensors," *Sensors*, **2017**.
29. G. Rodríguez, J. Casas and S. Villalba, "Cracking assessment in concrete structures by distributed optical fiber," *Smart materials and structures*, **2015**.
30. Y. Wang, B. Jin, Y. Wang, D. Wang, X. Liu and Q. Dong, "Distributed fiber-optic vibration detection system," in 2016 13th International Conference on Ubiquitous Robots and Ambient Intelligence, *URAI 2016*, **2016**.
31. E. Ruocco and V. Minutolo, "Buckling Analysis of Mindlin Plates Under the Green-Lagrange Strain Hypothesis," *International Journal of Structural Stability and Dynamics*, **2015**.
32. G. Uva, F. Porco, A. Fiore and G. Porco, "Structural monitoring using fiber optic sensors of a pre-stressed concrete viaduct during construction phases," *Case Studies in Nondestructive Testing and Evaluation*, **2014**.
33. B. Glisic, D. Hubbell, D. H. Sigurdardottir and Y. Yao, "Damage detection and characterization using long-gauge and distributed fiber optic sensors," *Optical Engineering*, **2013**.
34. Minardo, A., Catalano, E., Coscetta, A., Zeni, G., Zhang, L., Di Maio, C., Vassallo, R., Coviello, R., Macchia, G., Picarelli, L., Zeni, L. "Distributed fiber optic sensors for the monitoring of a tunnel crossing a landslide" *Remote Sensing*, 10 (8), 2018. DOI: 10.3390/rs10081291
35. Bernini, R., Fraldi, M., Minardo, A., Minutolo, V., Carannante, F., Nunziante, L., Zeni, L. "Identification of defects and strain error estimation for bending steel beams using time domain Brillouin distributed optical fiber sensors" *Smart Materials and Structures*, 15 (2), pp. 612-622, 2016, DOI: 10.1088/0964-1726/15/2/045.
36. Bernini, R., Minardo, A., Zeni, L. "Structural health monitoring by high-resolution Brillouin-based strain measurements", *Optics InfoBase Conference Papers*, 2006.
37. Bernini, R., Fraldi, M., Minardo, A., Minutolo, V., Carannante, F., Nunziante, L., Zeni, L. "Damage detection in bending beams through Brillouin distributed optic-fibre sensor, *Bridge Structures*, 1 (3), pp. 355-363, 2006.